Journal of Materials Chemistry C

Accepted Manuscript

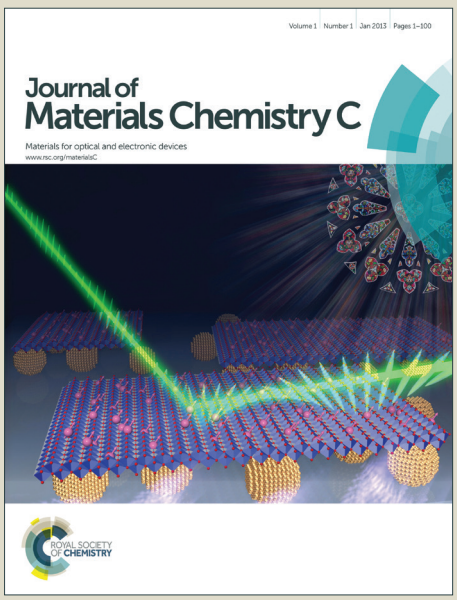

ROYAL SOCIETY OF CHEMISTRY

www.rsc.org/materialsC

Journal of Materials Chemistry C

RSCPublishing

ARTICLE

Carbon-encapsulated CdSe quantum dots inorganic hybrid nanobelts for high performance photoelectronic devices based on the efficient separation and transfer of photoinduced holes

Cite this: DOI: 10.1039/x0xx00000x

Received 00th January 2012,
Accepted 00th January 2012

DOI: 10.1039/x0xx00000x

www.rsc.org/

Jie Zhao,[a] Minghui Cao,[a] Baochang Cheng,[*,a,b] Guohong Wu,[a] Huijun Guo, [a] Yilong Ai,[a] Xiaohui Su,[b] Yanhe Xiao[a] and Shuijin Lei[a]

We developed a facile method of combustion synthesis followed by a selenylation process to synthesize carbon-encapsulated CdSe hybrid nanobelts. In the nanohybrids, hexagonal-wurtzite-structured CdSe quantum dots (QDs) are formed in situ and embedded uniformly in carbon nanobelt (CNB) matrix, resulting in the formation of an analogous p-i-n junction along the radial of QDs due to the appearance of inversion layer on the QD surfaces, which favors the separation of photoexcited electron-hole pairs by built-in electric field. Electrons accumulate in QD core, while holes migrate to QD surface and then quickly transfer to CNB matrix. Additionally, the nanohybrids can enhance significantly the absorption of the whole energy range of visible light. The nanohybrids can show p-type conductivity with hole mobility as high as 1.4×10^4 $cm^2V^{-1}s^{-1}$, and furthermore, the single nanohybrid-based devices not only show excellent photodetective performance at a certain bias, but also show photovoltaic-based self-powered photodetective performance at zero bias upon illuminating one end electrode of devices, pointing a way to the development of novel photoelectronic materials and devices for energy applications.

Introduction

CdSe is a vital member of II–VI group compounds and has attracted more and more attention for its advantage of suitable direct band gap (E_g=1.74eV), which gives it good response to visible light and a promising candidate for the application in photovoltaic and photoelectronic devices.[1-4] In recent decades, a lot of in-depth researches have been done on CdSe semiconductor quantum dots (QDs) due to their size-tunable band gap, photo-stability, relatively long excited state lifetime and unique shape dependent properties.[5-15] In particular, the multiple exciton generation makes it possible for the conversion efficiency of a QD-based single gap photovoltaic to reach 44.4%.[16] Therefore, it is highly desirable for CdSe QDs to serve as light harvesting materials in energy conversion devices. In spite of these promising properties, large quantities of grain boundaries produce surface states, which can trap photogenerated charges, and therefore, increase the probability of electron−hole recombination before charges being extracted by the electrodes.[17] As a result, the biggest challenge is still how to make effective separation of photogenerated electron-hole pairs and get them quickly transferred in CdSe QD-based optoelectronic devices. To enhance photoinduced charge separation and transfer, the formation of nanohybrids of QDs with one-dimensional (1D) nanostructure would be beneficial, for their small sizes and being ideal building blocks for these nanohybrid materials.[18]

For low-dimensional carbon allotropes such as carbon nanotube (CNT), and graphene, they can show high field-effect mobility and superior thermal conductivity. These fascinating properties hold promising potential for electronic devices, and chemical sensors.[19] For the zero-bandgap semiconductor, perfect graphene by itself does not show evident advantages in light-energy conversion application owing to its relatively short lifetime of excited states and small absorptivity throughout the visible spectral region.[20,21] However, low-dimensional carbon materials can act as supports to the QDs and transform the photoexcited states of the light-harvesting QDs into charge-separated states, have been widely used for combination with QDs to achieve efficient photovoltaic and sensitive photoconductive devices. Owing to large surface area and excellent carrier mobility, carbon allotropes are able to provide fast carrier transfer paths and prolong electron lifetime, which makes them suitable for applications in conductive network.[22] Some QD/carbon hybrids have been successfully used to collect and transport photoinduced charge carriers in photodetectors,[23-27] and photovoltaic devices.[28-30] To date, among various approaches reported for the synthesis of QD/carbon hybrids, it is not rarely seen QDs attached onto the surfaces of carbon materials by *in situ* growth,[31-34] or by direct combination via covalent or noncovalent bond.[35-40] The *in situ* growth, however, usually gives rise to the generation of highly polydispersed and inhomogeneous nanoparticles in shape and size. Moreover, if carbon nanomaterials were pretreated by chemical

modification, the intrinsic structure of carbon might be damaged to an extent, and its electric properties would be influenced. For the direct combination via a covalent bond, additionally, it is necessary to dispose the surfaces of either carbon materials or QDs to ensure their interconnection with each other, which might destroy the intrinsic properties and structure of carbon nanomaterials. In particular, some surfactant capping layers on the surface of QDs will block carrier transfer between QDs and carbon nanomaterials.[41] Therefore, it is still a huge challenge to develop low-dimensional carbon materials with novel structure in low cost, to serve as a carrier transport matrix for QDs-based devices, in which case photogenerated charges by the QDs get the advantage of being easily and quickly transferred to the carbon nanomaterials.[42-45]

Herein, we propose a new strategy to effectively control the photoresponse of CdSe semiconductors by deliberately designing 1D nanohybrid structure, for which CdSe QDs are formed *in situ*, and moreover, dispersed uniformly inside carbon nanobelt (CNB) matrix via a simple but effective technique of low-temperature combustion, followed by a selenylation process. In this way, QDs couple directly with carbon without any linker molecule or chemical modification of the CNBs, so that, the intrinsic properties of QDs and 1D nanostructure carbon can be preserved as much as possible. As revealed by the measurement of electric and optical properties, the nanohybrids showed an excellent performance with a high hole mobility and an effective energy transfer, and thus contributing to a high photoelectronic conversion efficiency. The approach mentioned above is not only very beneficial for the creation of highly efficient nano-electronic and nano-optoelectronic devices, but also opens a door for the application of 1D carbon materials.

Experimental Section

Synthesis of Carbon-Encapsulated CdSe Hybrid Nanobelts.

CdSe/carbon hybrid nanobelts were synthesized via a facile method of low-temperature combustion synthesis, followed by post-selenization. Typically, 0.03mol $Cd(NO_3)_2$ was dissolved in 15ml deionized water,and then 60ml triethanolamine was added to the cadmium nitrate aqueous solution. After mixing, the solution was placed in an oven at 150 ^oC for 6 h to remove the water. During this process, the mixture changes gradually from transparent to scarlet. Subsequently, the mixture was heated to about 280 ^oC, at which an auto-combustion reaction took place, and a black fluffy precursor was obtained. Finally, the precursor was placed at the middle of the ceramic tube in the furnace and then Se powder was located at about 5 cm upstream from the precursor. The selenylation reaction was carried out at 550 ℃, and held for 3 h in a weak reductive atmosphere of flowing 5% H_2 and 95% N_2 gas.

Structure Characterization of the as-Synthesized Hybrid Nanobelts.

The as-synthesized samples were characterized by X-ray diffraction (XRD, RIGAKU D/max-3b), field-emission environmental scanning electron microscopy (FE-ESEM, FEI Quanta 200F), and high-resolution transmission electron microscopy (HRTEM, JEOL 2100), respectively.

Measurement of Photoelectronic Properties.

The excitation density dependence of photoluminescence (PL) spectra was performed by the micro-PL system of a confocal laser micro-Raman spectrometer (LABRAM-HR, France JY Company) using the 514.5 nm line of an Ar^+ laser as an excitation source. The output power of laser is about 5 mW and the incident light is focused on a spot of about 5 um diameter by a microscopic objective. For the fluoresce image measurement of individual CdSe/carbon hybrid nanobelts, nanobelts were dispersed on a thin quartz substrate and then observed by a laser scanning confocal microscopy (LSCM, Zeiss LSM710) using a diode laser with a wavelength of 405 nm as an excitation source. The light emitted from the hybrid structures was collected by an objective lens. For the fabrication of the field effect transistor (FET), an individual hybrid nanobelt was transferred onto the surface of a degenerately doped silicon wafer with 300 nm dielectric of silicon dioxide. For the photocurrent and photovoltage detection experiments, an individual hybrid nanobelt was transferred on an Al_2O_3 substrate. The electrical contact was made by semi-dried silver paste at the two ends of the individual nanobelt. And then, a post-annealing under N_2 atmosphere at 400 °C for 10 min was applied to minimize the contact resistance. The micro-beam excitation light was given out by a microscope objective. The electric measurements were carried out by sourcemeter (Keithley 2400), synthesized function generator (Stanford Research System Model DS345), low-noise preamplifier (Stanford Research System Model SR560) and low-noise current preamplifier (Stanford Research System Model SR570). For the photodetective experiment of the spectral photoresponse vs wavelengths, the continuous wavelength light source was provided by a fluorescence spectrophotometer (Hitachi F4600) with a 150 W Xe lamp.

Results and Discussion

Morphology and Microstructure of as-Synthesized Nanohybrids

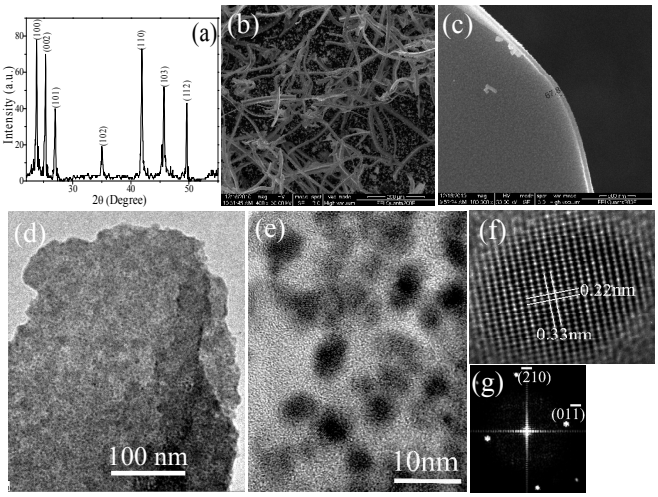

Fig. 1. Structural characterization of as-synthesized CdSe/CNB hybrids. (a) XRD pattern. (b) FE-SEM image. (c) high-magnification FE-SEM image of a single nanobelt, showing a thickness of about 70 nm. (d) TEM bright-field image of a single nanobelt, showing that QDs are uniformly dispersed in carbon matrix. (e) HRTEM image. (f) HRTEM image of a single QD. (g) The corresponding FTT analysis in (f).

The X-ray diffraction (XRD) pattern of as-synthesized nanohybrid is presented in Fig. 1a. All diffraction peaks whose values stand adjacently to that of reported (JCPDS file: 8-0459) in the Fig. can be indexed to the hexagonal-wurtzite-structured CdSe. No peaks of other phases are observed, indicating that carbon exists in amorphous form. Field-emission environmental scanning electron microscopy (FE-ESEM) images reveal the typical distribution of the

morphology for nanostructures, as shown in Fig. 1b and c. As can be seen, the samples mainly represent a belt-like shape with a thickness of about 100 nm. Shown in Fig. 1d is a typical low-magnification of bright-field transmission electron microscopy (TEM) image of a single nanobelt. It can be clearly seen that CdSe nanoparticles with an average diameter of about 5 nm are uniformly dispersed in carbon matrix. Fig. 1f displays a lattice-resolved TEM image of an individual QD, and the observed highly ordered interplanar spacings with *d*-values of about 0.33 and 0.22 nm correspond to $(01\bar{1})$ and $(\bar{2}10)$ planes of the wurtzite crystalline CdSe, respectively. The corresponding fast Fourier transform (FFT) analysis (Fig. 1g) can be indexed to hexagonal-wurtzite-structured CdSe with [122] zone axis.

Properties of Field Effect Transistor Based on Individual Hybrid Nanobelts

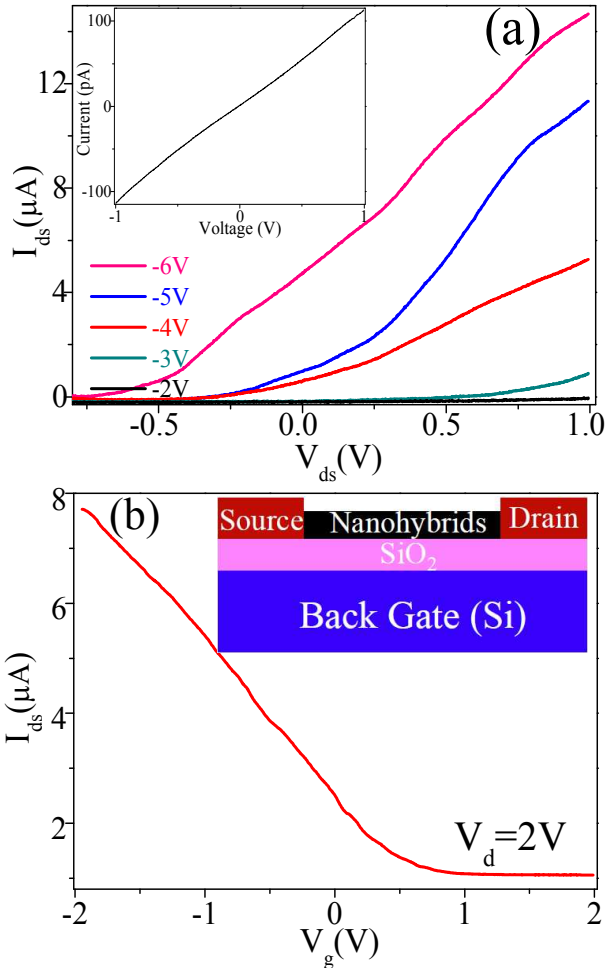

Fig. 2. (a) I_{ds}-V_{ds} curves of the CdSe/CNB hybrid FET recorded at different gate voltages, and the inset in (a) corresponds to *I-V* characteristic between source and drain. (b) I_{ds}-V_g curve of the hybrid nanobelt FET under V_{ds}=2 V, and the inset in (b) corresponds to the schematic configuration of FET device.

The field effect transistor (FET) device was constructed from a single hybrid nanobelt, and the electrical transport measurements were performed. The inset in Fig. 2b illustrates the structure of the FET device with the heavily doped p^+-Si substrate and the SiO_2 layer (300 nm) serving as the back-gate and the gate dielectric, respectively. The inset in Fig. 2a shows the *I-V* curve measured between the source and drain electrodes. It shows a linear behavior, confirming the ohmic contacts between the electrodes and the hybrid nanobet. As shown in Fig. 2a, the typical curves of source-drain current versus voltage (I_{ds}–V_{ds}) are obtained at varied gate voltages (V_g) from −2 V to -5 V by step of 1 V. It can be observed that the channel conductance of the hybrid nanobelt monotonously increases with applied negative V_g, and therefore, such gate voltage dependent I_{ds}–V_{ds} characteristics demonstrate the p-type conductivity of hybrids. Fig. 2b shows the corresponding transfer characteristics (I_{ds}-V_g), which depicts I_{ds}-V_g curve at V_{ds}=2 V. The hole concentration and mobility in hybrids can be estimated to be approximately 1.15×10^{14} cm^{-3} and 1.4×10^{4} $cm^2V^{-1}s^{-1}$, respectively basing on the experimental data.[46] The extremely large hole mobility implies a great potential for application in high-speed and high-frequency optoelectronic devices.

Excitation Intensity Dependence of Photoluminescence

Photoluminescence (PL) measurements have been extensively used to survey the separation efficiency of photogenerated charge carriers in a semiconductor because the recombination of an excited electron–hole gives rise to the PL emission signal.[47] The smaller the PL intensity is, the lower the recombination rate will be. In order to research the energy transfer properties in the nanohybrids, therefore, the excitation intensity dependence of the PL properties was measured at room temperature using the 514.5 nm line of an Ar^+ laser as an excitation source, and the results were presented in Fig. 3. The fluorescence image of a single hybrid nanobelt, taken by a laser scanning confocal microscopy (LSCM) and inset in Fig. 3c, further demonstrates that it can emit red light, which originates from the band-edge emission of CdSe. From Fig. 3a, it can be seen that PL spectra are composed of some relatively week peaks in range of 520~650 nm, related to the Raman scattering peaks of carbon, and a stronger band in range of 650~850 nm, associated with the band-edge emission of CdSe. In the enlargement, shown in Fig. 3b, the peaks located at around 1350, 1590, and 2800 cm^{-1} can be ascribed to D, G (E_{2g}), and 2D band of carbon-related Raman scattering, respectively. With increasing excitation intensity, their intensities increase while their positions are independent of excitation intensity and remain unchanged. For the red emission bands associated with the CdSe band-edge emission, which are magnified further and illustrated in Fig. 3c~f respectively, their intensities go up initially, reach a maximum at $0.5I_0$ excitation intensity, and then drop as the excitation density increases further. For the emission bands, however, their positions redshift gradually, and furthermore, their spectral widths enhance. More interestingly, the emission bands asymmetrically broaden on their high-energy sides, forming a typical Fano-like lineshape.[48-50] Moreover, the asymmetry enhances with an increase in excitation intensity.

Generally, the energy redshift and intensity reduction of band-edge emission are referred to as local heating effect as intense excitation laser illumination raises the sample temperature. In our case, the Raman scattering peaks, associated with carbon, do not show any measurable shift as the excitation power density varies. Therefore, the redshift and quenching of band-edge emission, related to CdSe, cannot be simply ascribed to the temperature increase due to the intense local heating induced by the Ar^+ laser.

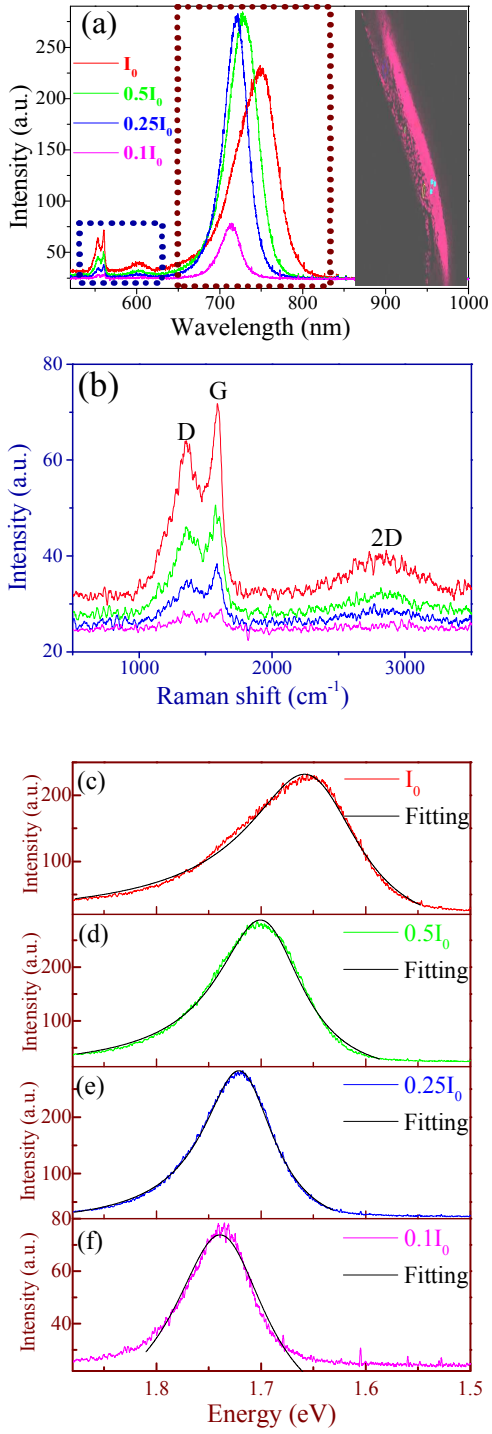

Fig. 3. PL spectra. (a) The excitation density dependence of room temperature PL spectra excited by an Ar^+ laser with a wavelength of 514 nm, and the insert in (a) is a fluorescent image of an individual CdSe/CNB hybrid measured by LSCM. (b) The enlargement of a navy doted frame in (a), corresponding to carbon-related Raman scattering. (c)-(f) The enlargement of a wine dotted frame in (a), corresponding to the band-edge emissions of CdSe at different excitation intensities and their asymmetric fitting curves by Fano interference effects (black curves).

Photoconductivity and self-Powered Photoconductivity

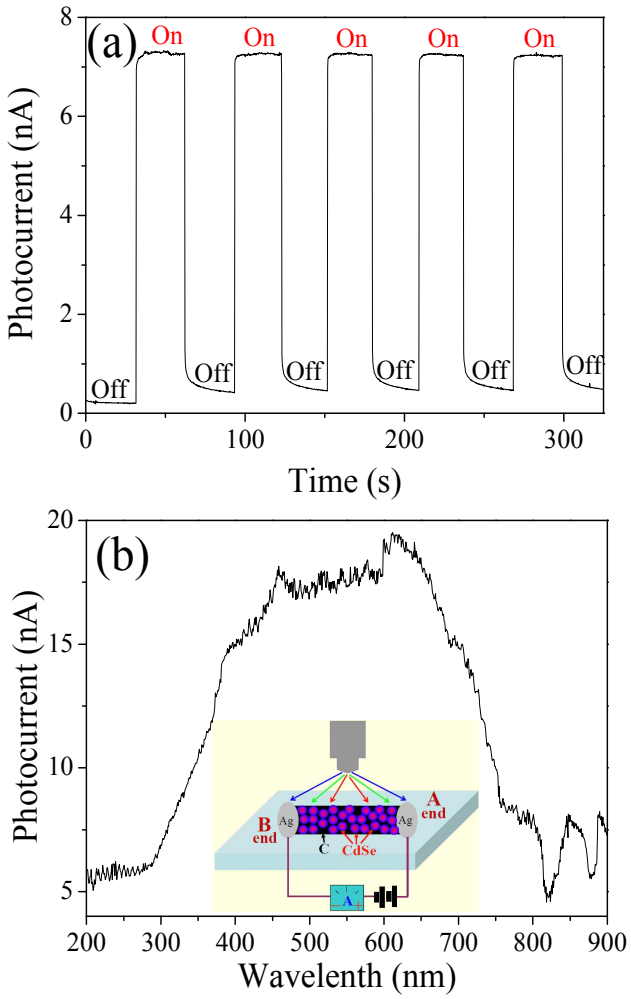

Fig. 4. Photoresponse of CdSe/CNB hybrid-based photodetector at 1V dc bias voltage. (a) The output signal of photocurrent under alternating light on and light off, where the entire device was illuminated by a visible light. (b) The spectral photoresponse vs wavelengths, showing a broad photoresponse range from 300 to 800 nm, that is, the absorption spectrum of the nanohybrid covers the whole energy range of visible light. (c) The corresponding schematic drawing of photodetector.

In order to understand the energy transduction pathway in more details and detect potential application in photoelectronic fields, we have performed further the experiments of photoconductivity at 1V dc bias and self-powered photoconductivity based on photovoltaic effect at zero bias, respectively, as shown in Fig. 4 and 5. As seen from Fig. 4a, the photocurrent increases at an applied dc bias voltage of 1 V. Moreover, the photoresponse is prompt, steady, and reproducible during repeated on/off cycles of the visible light illumination. More importantly, the nanohybrid-based device shows a very broad photoresponse range from 300 to 800 nm, as shown in Fig. 4b, and therefore, the nanohybrid can harvest the whole energy range of visible light. Based on the above analysis of FET characteristics, the majority charge carriers are holes in the CdSe/CNB hybrid system. Upon light excitation, and therefore, the photoconductivity effect originates from the increase of hole concentration in carbon matrix, donated by the holes transfer from QDs by photovoltaic separation effect. At zero bias, one end of the Ag-CdSe/C-Ag device is illuminated with a micro-beam visible light from an optical microscopy objective, as shown in Fig. 5. It can be

clearly seen that the device shows the potential of 0.13 mV between the two electrodes at both ends, and additionally, the voltage of the end subjected to the light illumination, is negative while that of the other is positive. This result not only confirms further that the hole concentration increases significantly in CNB matrix upon visible light illumination, but also indicates the reduction of the recombination of electron–hole pairs in QDs. The photogenerated holes can transfer and transport to the other end along 1D CNB, resulting in a presence of higher potential in the end without illumination. The appearance of potential difference between the both ends generates self-powered photoconductivity effect. This result also demonstrates embedded QDs can efficiently harvest visible light, and moreover, photoexcited electron-hole pairs can be effectively separated by the built-in electric field of p-i-n junction formed in QDs. In addition, CNB matrix can serve as a good conducting scaffold to collection and transport hole carriers transferred from QDs. The single hybrid nanobelts can yield a notable photovoltaic effect by itself, indicating that the carbon-based nanohybrids have promising potential applications in solar-energy conversion for photovoltaic cells and self-powered photodetectors.

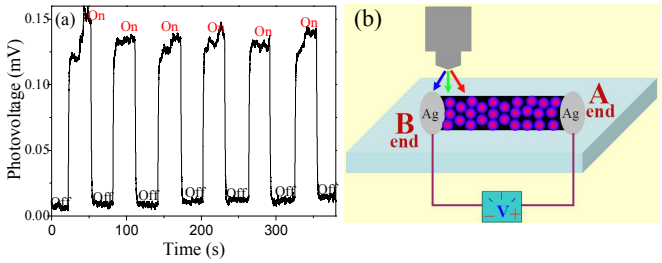

Fig. 5. Self-powered photodetector of CdSe/CNB hybrid based on photovoltaic effect at zero bias voltage. (a) The output signal of photovoltage under alternating light on and light off. The end which is connected to the cathode of voltmeter is illuminated by a micro-beam visible light. (b) The corresponding schematic diagram of testing device.

Mechanism of Photoinduced Energy Transfer and Asymmetric PL

It is generally accepted that excited state QDs are deactivated (quenched) by carbon allotropes via energy transfer. At higher excitation intensity, the quenching of PL indicates a notable lower recombination rate or a more efficient separation and transfer of photogenerated charge pairs between QDs and carbon matrix, and the lifetime of charge carriers was efficiently lengthened. For the energy transfer, the two mechanisms of Förster-type dipole-dipole interaction (Förster resonance energy transfer, FRET) and photoinduced charge transfer (CT) have been proposed.[13-15,51] For the CT process, electrons directly transfer from QDs to carbon matrix, leading to a decrease of hole concentration in carbon matrix.[52-55] Although the majority charge carriers would be electrons donated from CdSe QDs,[56,57] the FET characteristics of nanohybrid-based devices demonstrate a p-type semiconductor property where the positively charged holes are the majority charge carriers, and moreover, the photoconductive experiment results demonstrate an increase of hole concentration in nanohybrids upon visible light illumination. The photoinduced energy transfer in carbon-encapsulated CdSe hybrid nanobelts, therefore, cannot be simply attributed to photoinduced electron transfer mechanism.

The energy level diagram of the device is presented in Fig. 6. The conduction band (CB) edge of the CdSe QDs can be estimated to be approximately -4.0 eV from the electron affinity and ionization potential of bulk CdSe,[58,59] with a correction for the quantum size effect.[60] The reported work function of carbon is about 5 eV,[61] placing its Fermi level (E_f) between the valence band (VB) and CB of CdSe QDs, as shown in Fig. 6a. For CdSe, it is typical n-type semiconductor,[56,57] and therefore, its E_f is higher than that of carbon. When CdSe QDs contact with CNB matrix each other, electrons will diffuse from CdSe QDs to CNB, then their energy bands bend near their interface, and finally their E_f will reach the same magnitude. For CNBs, the shift of E_f is negligible due to high density of carriers and relatively large volume as compare with QD. For a single CdSe QD, the total number of free electrons is limited, and the shift of free electrons from QD to CNB results in a drastic reduction of electron concentration. Therefore, the E_f will be away from the CB, and the region close to the core will be almost depleted completely, and moreover, electron trap states will also be emptied. In particular, the E_f of surface layer will be lower than the intermediate level (E_i), that is, the surface layer will form an inversion layer and transform into p-type, as shown in Fig. 6b. As a result, an analogous p-i-n junction will be formed along the radial of individual QDs. When the nanohybrids are illuminated by the visible light with energy above the band gap energy of CdSe, quantities of electron-hole pairs will be generated, and then can be separated effectively by the built-in electric field of p-i-n junction. Electrons will migrate and accumulate into QD core, resulting in a charged state. Moreover, electron trap states will also be filled up. Correspondingly, E_f will be close to CB, and the width of the intermediate depletion layer will become narrow. However, photogenerated holes will migrate to surface p-type inversion layer and then will quickly transfer to CNB matrix, resulting in the generation of photocurrent. When an end of hybrid nanobelt is illuminated by a visible light, therefore, the potential of other one will rise, namely the the generation of photovoltage. The corresponding schematic diagrams of energy level and charge transfer are illustrated in Fig. 6c.

The asymmetric lineshape implies the presence of a Fano-like interference between discrete and continuum states in PL spectra.[17] Without or low excitation intensity, the intermediate depletion layer is relatively wide, and therefore, the excitations should be discrete interband excitons, mainly originating from depletion region. With increasing excitation intensity, the width of depletion region decreases, and quantities of electrons will accumulate in QDs core region, resulting in charged state, and furthermore, electron trap states are also filled up. High density of free electrons induces E_f to rise above CB level, resulting in the formation of degenerate state. The incident light with energy above QD band gap energy can be efficiently absorbed. Moreover, PL emission will change from exciton annihilation into the electron transition between trap levels and VB,[62,63] and therefore, the position of emission peak exhibits a distinct redshift with increasing in excitation intensity. Additionally, the accumulation of quantities of free electrons results the formation of plasmons. The coupling between the continuum plasmons and the discrete excitations can lead to a nonlinear Fano effect,[48-50,64] which make PL emission peak asymmetrically broaden on its high-energy side. With increasing excitation intensity, moreover, the depletion region width decreases, and the plasmon concentration increases dramatically in QD core due to a more efficient separation of photogenerated electron-hole pairs. Therefore, the stronger coupling results in a more striking asymmetry of the PL emission band. In order to quantitatively analyze the above-mentioned effects, the experimental data of hybrid exciton emission are theoretically fitted with Fano line-shape given by:[50]

$$I(\omega) = A\frac{(q+\varepsilon)^2}{(1+\varepsilon^2)} \quad \text{and} \quad \varepsilon = \frac{(E-E_0)}{\Gamma}$$

Where E_0 is the renormalized or "dressed" photon energy in the presence of the coupled emission, Γ is the line-width parameter, and q is the asymmetry parameter ($1/q$ is referred to as the coupling strength). The interaction between discrete excitations and continuum plasmons is determined by q. A small value of q implies a much stronger interference effect. The fitting results show that q value is respectively 5.52, 9.44, 11.34, and 23.5 at the excitation intensity of I_0, $0.5I_0$, $0.25I_0$, and $0.1I_0$. It can be obviously seen that $1/q$ increases as the power density of the incident laser increases, indicating that there is constructive interference between the discrete photon and continuum plasmons on the high-energy and destructive interference on the low-energy side, and moreover, the coupling strength increases with increasing excitation density.

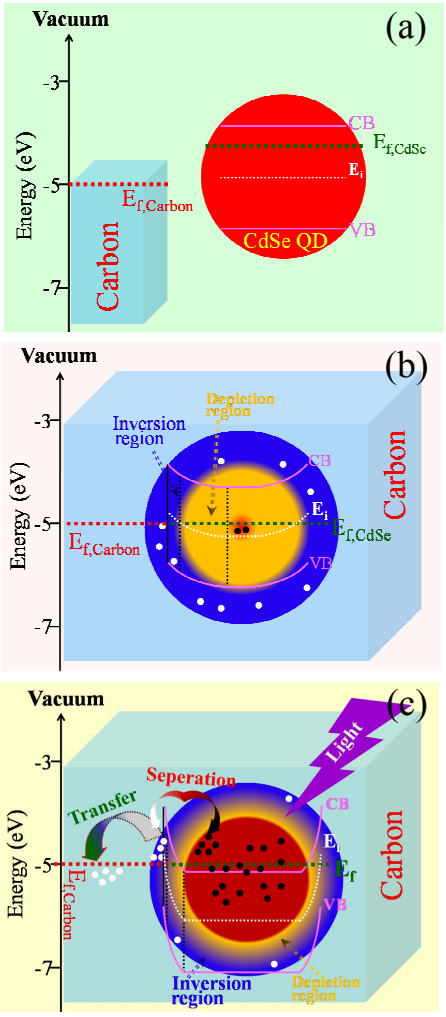

Fig. 6. Schematic diagrams of energy level and photoinduced charge transfer between CdSe QD and CNB matrix. (a) CdSe QD and CNB matrix are noncontact, showing independent energy levels. (b) QD is embedded into CNB matrix without light illumination. The diffusion of electrons into carbon results in the formation of an inversion layer near the QD surface and an almost complete depletion region close to the QD core, namely, the formation of analogous p-i-n junction along the radial of QD. (c) QD is embedded into CNB matrix with light illumination. Photoexcited electron-hole pairs can be effectively separated by the built-in electric field of p-i-n junction in QD. Thus, electrons accumulate in QD core, while holes migrate to QD surface and then transfer to CNB matrix.

Conclusions

In summary, we have developed a simple but effective method of combustion synthesis followed by a selenylation process to synthesize carbon-encapsulated CdSe hybrid nanobelts, in which case CdSe QDs are formed *in situ* and dispersed uniformly in the CNB matrix. There is a significant interaction between the CdSe QDs and the CNB interface. The 1D carbon nano-encapsulating works in multiple ways, providing protection of the QDs surface, enhancing light absorption range and efficiency, and facilitating the energy transport from QDs to CNBs. The synergistic effect between CdSe QDs and CNB nano-encapsulating was systematically investigated by the measurement of the electric transport and the excitation power dependence of PL. The resultant 1D nanohybrids show an excellent p-type electric property with the hole mobility as high as 1.412×10^4 cm^2 V^{-1} s^{-1}. In the hybrid structure, additionally, the formation of an analogous p-i-n junction along the radial of QDs provides an efficient pathway for the separation of photogenerated electron-hole pairs. Therefore, in the nanohybrids, QDs, served as light harvester, can absorb the whole energy range of visible light, and then efficiently transfer photoinduced holes to CNB matrix by the built-in electric field separation of p-i-n junction. On the basis of photovoltaic separation effect, the individual nanohybrid-based devices can not only show an excellent photodetective performance at a certain bias upon illuminating the entire nanobelt between both end electrodes, but also show a self-powered photodetective performance at zero bias upon illuminating one end of individual hybrid nanobelts. It is believed that this synthesis method can be extended to prepare a wide variety of functional nanohybrids for different applications. In addition, the nanohybrids that we have shown here not only are useful for the creation of highly efficient optoelectronic devices, but also provide an alternative route for the application of 1D carbon materials.

Acknowledgements

This work was supported by the National Natural Science Foundation of China (21263013, 51162023, 51462023), the Project for Young Scientist Training of Jiangxi Province (20133BCB23002), the Natural Science Foundation of Jiangxi Province (20132BAB206005, 20114BAB206027) and the Foundation of Jiangxi Educational Committee (GJJ13058).

Notes and references

[a] School of Materials Science and Engineering, Nanchang University, Jiangxi 330031, P. R. China
[b] Nanoscale Science and Technology Laboratory, Institute for Advanced Study, Nanchang University, Jiangxi 330031, P. R. China

1 L. H. Zhang, Y. Jia, S. S. Wang, Z. Li, C. Y. Ji, J. Q. Wei, H. W. Zhu, K. L. Wang, D. H. Wu, E. Z. Shi, Y. Fang, A. Y. Cao, *Nano Lett.* 2010, **10**, 3583.
2 M. Bruchez, M. Moronne, P. Gin, S. Weiss, A. P. Alivisatos, *Science* 1998, **281**, 2013.
3 J. H. Bang, P. V. Kamat, *Acs Nano*, 2009, **3**, 1467.
4 Z. F. Feng, Q. B. Zhang, L. L. Lin, H. H. Guo, J. Z. Zhou, Z. H. Lin, *Chem. Mater.* 2010, **22**, 2705.
5 S. A. McDonald, G. Konstantatos, S. Zhang, P. W. Cyr, E. J. D. Klem, L. Levina, E. H. Sargent, *Nat. Mater.* 2005, **4**, 138.
6 G. Konstantatos, I. Howard, A. Fischer, S. Hoogland, J. Clifford, E. Klem, L. Levina, E. H. Sargent, *Nature* 2006, **442**, 180.
7 G. Konstantatos, J. Clifford, L. Levina, E. H. Sargent, *Nat. Photon.*

2007, **1**, 531.
8 V. Sukhovatkin, S. Hinds, L. Brzozowski, E. H. Sargent, *Science* 2009, **324**, 1542.
9 J. P. Clifford, G. Konstantatos, K. W. Johnston, S. Hoogland, L. Levina, L.E. H. Sargent, *Nat. Nanotechnol.* 2009, **4**, 40.
10 G. Konstantatos, E. H. Sargent, *Nat. Nanotechnol.* 2010, **5**, 391.
11 Y. Y. Wang, Y. H. Liu, Y. Zhang, F. D. Wang, P. J. Kowalski, H. W. Rohrs, R. A. Loomis, M. L. Gross, W. E. Buhro, *Angew. Chem. Inter. Ed.* 2012, **51**, 6154.
12 S. Jun, E. Jang, *Angew. Chem. Inter. Ed.* 2013, **52**, 679.
13 Z. Y. Chen, S. Berciaud, C. Nuckolls, T. F. Heinz, L. E. Brus, A*CS nano* 2010, **4**, 2964.
14 M. H. Stewart, A. L. Huston, A. M. Scott, E. Oh, W. R. Algar, J. R. Deschamps, K. Susumu, V. Jain, D. E. Prasuhn, J. Blanco-Canosa, P. E. Dawson, I. L. Medintz, *ACS nano* 2013, **7**, 9489.
15 S. R .Guo, D. D. Bao, S. Upadhyayula, W. Wang, A. B. Guvenc, J. R. Kyle, H. Hosseinibay, K. N. Bozhilov, V. I. Vullev, C. S. Ozkan, M. Ozkan, *Adv. Funct. Mater.* 2013, **23**, 5199.
16 M. C. Hanna, A. J. Nozik, *J. Appl. Phys.* 2006, **100**, 074510.
17 D. Wang, J. K. Baral, H. Zhao, B. A. Gonfa, V. V. Truong, M. A. El Khakani, R. Izquierdo, D. Ma, *Adv. Funct. Mater.* 2011, **21**, 4010.
18 V. Georgakilas, D. Gournis, V. Tzitzios, L. Pasquato, D. M. Guldi, M. J. Prato, *Mater. Chem.* 2007, **17**, 2679.
19 K. I. Bolotin, K. J. Sikes, Z. Jiang, M. Klima, G. Fudenberg, J. Hone, P. Kim, H. L. Stormer, *Solid State Commun.* 2008, **146**, 351.
20 K. F. Mak, M. Y. Sfeir, Y. Wu, C. H. Lui, J. A. Misewich, T. F. Heinz, *Phys. Rev. Lett.* 2008, **101**, 196405.
21 R. R. Nair, P. Blake, A. N. Grigorenko, K. S. Novoselov, T. J. Booth, T. Stauber, N. M. R. Peres, A. K. Geim, *Science* 2008, **320**, 1308.
22 S. Sun, L. Gao, Y. Liu, J. Sun, *Appl. Phys. Lett.* 2011, **98**, 093112.
23 N. Cho, K. Roy Choudhury, R. B. Thapa, Y. Sahoo, T. Ohulchanskyy, A. N. Cartwright, K. S. Lee, P. N. Prasad, *Adv. Mater.* 2007, **19**, 232
24 B. Zebli, H. A. Vieyra, I. Carmeli, A. Hartschuh, J. P. Kotthaus, A. W. Holleitner, *Phys. Rev. B* 2009, **79**, 205402.
25 X. Li, Y. Jia, A. Cao, *ACS Nano* 2010, **4**, 506.
26 H. C. Shim, S. Jeong, C. S. Han, *Nanotechnology* 2011, **22**, 165201.
27 I. Ka, V. Le Borgne, D. Ma, M. A. El Khakani, *Adv. Mater.* 2012, **24**, 6289.
28 I. Robel, B. A. Bunker, P. V. Kamat, *Adv. Mater.* 2005, **17**, 2458.
29 A. Kongkanand, R. Martínez Domínguez, P. V. Kamat, *Nano Lett.* 2007, **7**, 676.
30 X. Li, Y. Jia, J. Wei, H. Zhu, K. Wang, D. Wu, A. Cao, *ACS Nano* 2010, **4**, 2142.
31 I. Robel, A. B. Bunker, P. V. Kamat, *Adv. Mater.* 2005, **17**, 2458.
32 S. Banerjee, S. S. Wong, *Chem. Commun.* 2004, 1866
33 B. H. Juarez, C. Klinke, A. Kornowski, H. Weller, *Nano Lett.* 2007, **7**, 3564.
34 Y. J. Na, H. S. Kim, J. Park, *J. Phys. Chem. C* 2008, **112**, 11218.
35 S. Banerjee, S. S. Wong, *Nano Lett.* 2002, **2**, 195.
36 L. Sheeney-Haj-Ichia, B. Basnar, I. Willner, *Angew. Chem., Int. Ed.* 2005, **44**, 78.
37 C. Lu, A. Akey, W. Wang, I. P. Herman, *J. Am. Chem. Soc.* 2009, **131**, 3446.
38 M. Olek, T. B€usgen, M. Hilgendorff, M. Giersig, *J. Phys. Chem. B* 2006, **110**, 12901.
39 X. Peng, S. S. Wong, *Chem. Mater.* 2009, **21**, 682.
40 J. E. Weaver, M. R. Dasari, A. Datar, S. Talapatra, P. Kohli, *ACS Nano* 2010, **4**, 6883.
41 Z. Shi, C. S. Liu, W. H. Lv, H. B. Shen, D. Wang, L. W. Chen, L. S. Li, J. Jin, *Nanoscale*, 2012, **4**, 4515.
42 P. Avouris, Z. Chen, V. Perebeinos, *Nat. Nanotechnol.* 2007, **2**, 605.
43 A. N. Cao, Z. Liu, S. S. Chu, M. H. Wu, Z. M. Ye, Z. W. Cai, Y. L. Chang, S. F. Wang, Q. H. Gong, Y. F. Liu, *Adv. Mater.*, 2010, **22**, 103.
44 B. Farrow, P. V. Kamat, *J. Am. Chem. Soc.* 2009, **131**, 11124.
45 P. Brown, P. V. Kamat, *J. Am. Chem. Soc.*, 2008, **130**, 8890.
46 R. Martel, T. Schmidt, H. R. Shea, T. Hertel, P. Avouris, *Appl. Phys. Lett.* 1998, **73**, 2447.
47 G. Itskos, A. Othonos, T. Rauch, S. F.Tedde, O. Hayden, M. V. Kovalenko, W. Heiss, S. A. Choulis, *Adv. Energy Mater.* 2011, **1**, 802.
48 U. Fano, *Phys. Rev.* 1961, **124**, 1866.
49 R. Gupta, Q. Xiong, C. K. Adu, U. J. Kim, P. C. Eklund, *Nano Lett* .2003, **3**, 627.
50 F. Cerdeira, T. A. Fjeldly, M. Cardona, *Phys. Rev. B* 1973, **8**, 4734.
51 M. H. Stewart, A. L. Huston, A. M. Scott, E. Oh, W. R. Algar, J. R. Deschamps, K. Susumu, V. Jain, D. E. Prasuhn, J. Blanco-Canosa, P. E. Dawson, I. L. Medintz, *ACS Nano*, 2013, **7**, 9489.
52 L. B. Hu, Y. L. Zhao, K. Ryu, C. Zhou, J. F. Stoddart, G. Gruner, *Adv. Mater.* 2008, **20**, 939.
53 B. H. Juaraz, C. Klinke, A. Kornowski, H. Weller, *Nano Lett.* 2007, **7**, 3564.
54 G. Mountrichas, A. S. D. Sandanayaka, S. P. Economopoulos, S. Pispas, O. Ito, T.Hasobe, N. Tagmatarchis, *J. Mater. Chem*. 2009, **19**, 8990.
55 S. Leubner, G. Katsukis, D. M. Guldi, *Faraday Discuss.* 2012, **155**, 253.
56 S. Y. Jeong, S. C. Lim, D. J. Bae, Y. H. Lee, H. J. Shin, S. M. Yoon, J. Y. Choi, O. H. Cha, M. S. Jeong, D. Perello, M. Yun, *Appl. Phys. Lett.* 2008, **92**, 243103.
57 Rajesh, T. Sarkar, A. Mulchandani, *Appl. Phys. Lett.* 2011, **99**, 173110.
58 S. H. Kim, G. Markovich, S. Rezvani, S. H. Choi, K. L. Wang, J. R. Heath, *Appl. Phys. Lett.* 1999, **74**, 317.
59 T. C. Chiang, F. J. Himpsel, Landolt-Börnstein, *New Series III/23a*, 1989, **95**.
60 L. E. Brus, *J. Chem. Phys.* 1996, **79**, 2745.
61 D. R. Lide, *CRC Handbook of Chemistry and Physics version*, CRC Press, 2008.
62 X. F. Han, Y. X. Weng, A. L. Pan, B. S. Zou, J. Y. Zhang, *Appl. Phys. Lett.* 2008, **92**, 032102.
63 S. Yamaguchi, H. Kurusu, Y. Kawakami, S. Fujita, *Phys. Rev. B* 2000, **61**, 10303.
64 W. Zhang, A. O. Govorov, G. W. Bryant, *Phys. Rev. Lett.* 2006, **97**, 146804.